INTERNATIONAL JOURNAL OF PRECISION ENGINEERING AND MANUFACTURING Vol. 15, No. 10, pp. 2077-2084 OCTOBER 2014 / 2077
DOI: 10.1007/s12541-014-0566-8

Dynamic Modeling of Coupled Tendon-Driven System for Surgical Robot Instrument

Chi Yen Kim[1], Min Cheol Lee[2,#], Ryan Blaine Wicker[1], and Sung-Min Yoon[2]

1 Department of Mechanical Engineering, The University of Texas at El Paso, 500 W. University Ave, El Paso, Texas, USA, 79968
2 School of Mechanical Engineering, Pusan National University, San 30, Jangjeon-dong, Geumjeong-gu, Busan, South Korea, 609-735
Corresponding Author / E-mail: mclee@pusan.ac.kr, TEL: +82-51-510-2439, FAX: +82-51-512-9835

KEYWORDS: Manipulator dynamics, Tendon-driven, Surgical robot instrument

This paper is the study of a surgical instrument which directly performs MIS(Minimally Invasive surgery) on a patient, instead of a surgeon. The instrument used in robot assisted laparoscopy adopts a tendon driven mechanism so that it generates hand-like surgical motion through aperture of trocar. To create a high DOF of motion in restricted spaces, cable systems for end-effector have been organized by serial kinematic chains which can cause interference among joints sharing same axis. Also, to prevent the elongation of any cable, composited and pre-extended cables, which show nonlinear characteristics, are used in surgical instrument tendon system. As aforementioned difficulty and complexity, there are not many studies about measuring or estimating the operating force of instruments without sensors, which is needed for safety but still impossible in commercial systems. This paper derives governing a dynamic model of a coupled cable pulley structure while considering the material tensile characteristics of the cables. The derived model can estimate the operating force on end-effector as well as states of all inner pulleys without encoders. This paper proves the availability of proposed methodology with comparison of numerical analysis and the experimental test of 2 DOF serial kinematic chained cable pulley link apparatus.

Manuscript received: October 4, 2012 / Revised: May 29, 2014 / Accepted: June 2, 2014

NOMENCLATURE

MIS = minimally invasive surgery
LAS = laparoscopic assisted surgery
J_m = inertia of driving motor for end-effector
J_L = inertia of driving motor for link
J_i = inertia of inner pulleys and link
B_m = damping ratio of driving motor for end-effector
B_L = damping ratio of driving motor for link
B_i = damping ratio of inner pulleys and link
$\overline{T}_{m1}$ = tension between pulley M and 1
$\overline{T}_{12}$ = tension between pulley 1 and 2
$\overline{T}_{L3}$ = tension between pulley L and 3
$K(\delta)$ = spring rate function with elongation
δ = elongation

1. Introduction

Minimally invasive surgery (MIS) and laparoscopic-assisted surgery (LAS) have become alternatives to traditional open surgery because much of the pain of recovery and length of hospitalization can be reduced by eliminating large incisions and extensive dissection.[1] With advances in robot technologies, a surgical robot was developed for MIS to make it possible to penetrate complex and deep organs in the body and to properly operate without exposing internal organs to possible external contaminants owing to the multiple degree of freedom (DOF) merits of the robot. This produced good results in terms of fast recovery with low pain and a lower infectious rate then general open invasive surgery.[2]

Laparoscopy, whether conventional or robot-assisted, mainly involves an instrument used for performing operations inside the body; this instrument is manipulated by motion, and power is transmitted from outside the body. The principle of levers, like scissor shapes or trigger structures, has been used in conventional laparoscopic instruments as an operating mechanism. A rigid frame transmits the power and movement. These methods have merit in that when gripping

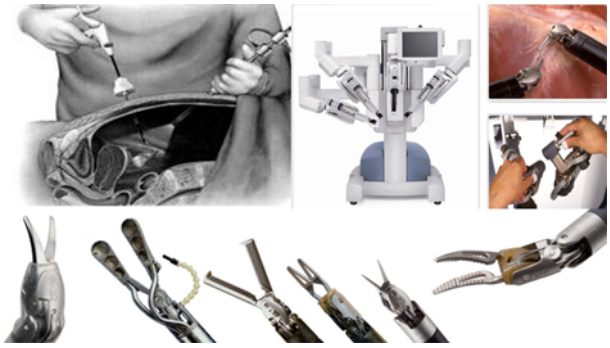

Fig. 1 Conventional laparoscopic surgery, robot-assisted laparoscopic surgery (Da Vinci Surgical robot) and various instrument tips (Endowrist)

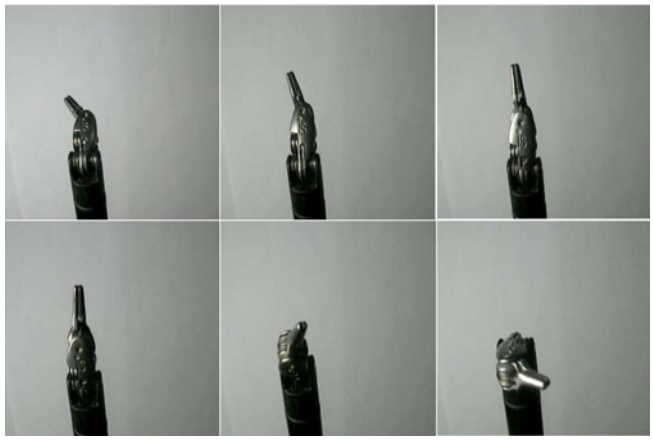

Fig. 2 Posture change of forceps caused by wrist rotation

or pulling the organ, the surgeon can feel the operating force through the reflected reaction force. However, a straight and simple structure restricts the available DOF. To increase the working DOF, many structures have been developed, e.g., rotaTable and bendable structure. However, these improvements cannot satisfy the difficulties of instrument penetration according to the type of surgery.[3-5]

As D.A.G. Reyes, B. Tang and A. Cuschieri[6] demonstrated, a limited DOF and surgeon-instrument interface can degrade spatial perception, which causes surgeons to require long periods of practice and induces stress and fatigue. S. Horgan and D. Vanuno showed that a robot-assisted laparoscopic system reduces these problems, and they forecasted an expansion in its usage.[7]

Robot systems for laparoscopic surgery have a master-slave manipulator system to enable surgeons to have stress-free interaction with the surgical workspace and to conduct precise surgical operations with a high DOF using a robot arm and instrument driving control. As the instrument used in robot-assisted laparoscopy requires a higher DOF than conventional laparoscopy, several mechanisms have been researched to generate a high DOF for MIS.[8,9] However, by law, the surgical robot instrument has to be discarded after being used a certain number of times to reduce the risk of infection. As they have to be small for MIS and cost little for disposal, most commercial surgical robot instruments, e.g., EndoWrist, which is used in the Da Vinci robot of Intuitive Surgical. Inc, adopt a tendon-driven mechanism using a cable and pulley system.[10]

The cable-pulley system uses tension based on the elasticity of the cable; thus, it is difficult to control the force of the surgical robot instrument simply by assuming a rigid body model. Furthermore, minimizing the size can cause interference. As surgical robot instruments perform operations directly inside the body, precise control of the motion and force control during gasping or pushing are required, especially when the tip goes out of view. At present, as it is difficult to control the operating force as well as to obtain force feedback during the operation, surgeons perform robot-assisted surgery simply by presuming the state using endoscope vision. Thus, they need long-term practice to avoid accidents, like breaking needles, cutting threads, and hurting organs.[17] For safe and precise control, a system dynamic model is required. Thus, this paper presents the dynamic model for a surgical instrument that considers the nonlinear elasticity characteristics of a cable and coupled motion.

Instead of the surgical robot instrument field, the tendon-driven mechanism was examined using control theory[11] and using the practical application of haptic or hand posture.[12] In an early study on the mechanism in Ref. 13 the dynamic model was based on constant stiffness. In 2006, Yin studied the limitations in the performance of a tendon-driven mechanism based on cable yielding.[14] Recently, variable stiffness in the cable has been considered to solve the system torque and stiffness equation.[11] Surgical robot instruments use a pre-extended cable to reduce elongation;[15] in a previous study, the nonlinear characteristics of a pre-extended cable were shown to make indirect measurement of the reaction force possible by using a moving plate and load cell.[16]

This study examined a representative cable-driven model for a surgical robot instrument to determine a dynamic model that considers nonlinear variable stiffness and coupled motion. In the next section, an analysis of the tendon-driven system in surgical robot instrument is presented for investigating the material characteristics of cables used in a surgical robot instrument and for deriving a dynamic model. In section, the derived model was validated by simulation and experiment. The conclusions are given in the final section.

2. Dynamic Analysis

2.1 Tendon-driven system in surgical robot instruments

Minimal invasive surgery (MIS) is conducted by inserting an instrument through a small punched hole. The incision size is so small that the pain of recovery, risk of infection, and the length of hospitalization are reduced, unlike the inescapably large incision and extensive dissection of traditional open surgery. Therefore, the surgical robots and operation instruments used in MIS have to be as small as possible. For the safety of the patient, there is also a law that states that the parts of an operation instrument used inside a body must be scrapped after a certain number of uses. Thus, cost becomes a factor. Both of the above issues are solved by adopting tendon-driven mechanism in surgical robot instruments.

However, the tendon-driven mechanism has a few systemic drawbacks as well as control complexity. First, it makes a coupled motion. There is some interference as several pulleys are installed on

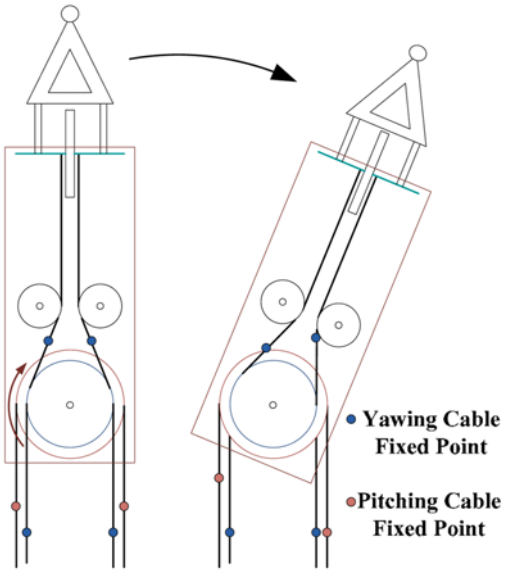

Fig. 3 Posture change of forceps caused by wrist rotation

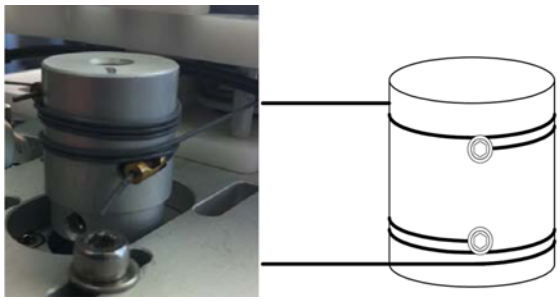

Fig. 4 Pull-pull structure to prevent slip on pulley

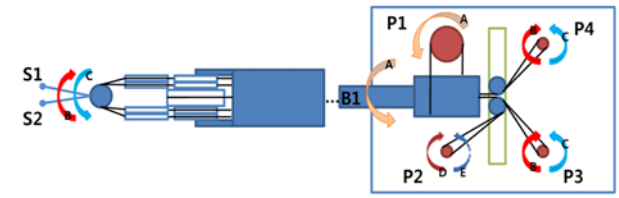

(a) Planar figure of end-effector tip and driving pulleys

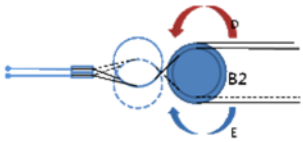

(b) Lateral figure of end-effector tip

Fig. 5 Movement of instrument tip and driving pulleys

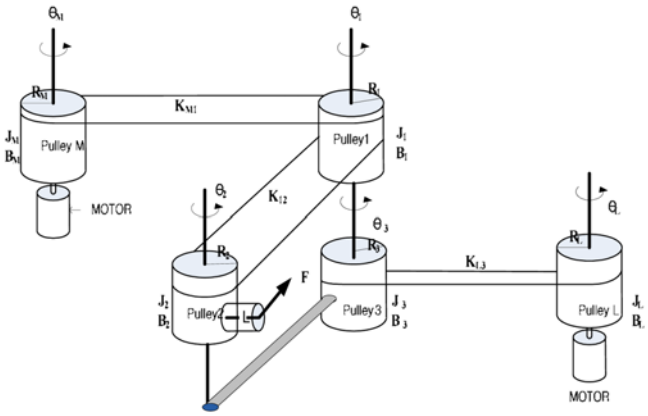

Fig. 6 Basic structure of a 2 DOF tendon-driven systems

the same shaft to reduced the size. Fig. 2 shows the interference phenomenon for the Endowrist instrument used in the Da Vinci robot. Although the driving motors of fingertips are fixed, the fingers are rotated as the wrist moves. The interference occurs because the lower link pulley rotation causes a relative rotation in the idle upper link pulley installed on the same shaft, as shown in Fig. 3. Therefore, the trajectory for multiple DOFs should be generated by considering the coupled effect.

General cable-pulley systems have slag and slip problems. Most surgical robot instruments adopt pull-pull structures, as shown in Fig. 4, to avoid the slip problem. To avoid slip on the pulleys, a couple of the cables are wound and fixed on pulleys in opposite directions. As the slag phenomenon occurs by clearance originating from the elasticity and surplus cable length, surgical robot instruments are loaded with pretension to reduce the loose effect. However, previous research has shown that raising the pretension generates an increase in friction.[18] Thus, instead of the rigid body model adopted for general robot systems, the system dynamic model for a surgical robot instrument should consider the coupled structure and elasticity characteristics of a pre-extended cable.

2.2 Governing equation

The governing equation is derived here; it includes the torque of the driving motor part, the motion of multiple idle pulleys, and the operation force on the end-effector of in a surgical robot instrument.

In addition, it can estimate the reaction force by applying the observer force using control theory. To derive the governing equation, the structure of a general surgical robot instrument should be understood first. The general surgical robot instrument basically simulates the motion of a surgeon's two fingers; the thumb and index finger. Therefore, the instrument consists of two fingers and an additional two DOFs for the fingers, pitching and rolling as shown in Fig. 5. The rolling motion is normally conducted by rotating the entire tube of the instrument to avoid system complexity and additional interference. The pitching and grasping function machinery is built at the end part of the instrument for compactness. To reduce the size, the pulley for the fingertip is built on the pitching link in series. The grasping motion is generated by the relative rotation of the two fingertips. Thus, the basic inner structure of the instrument can be summarized as two DOFs; one finger moves by rotating and pitching. Fig. 6 shows the structure. In the Fig., notation M and L are driving pulleys for end-effector and pitching link respectively. The digit notations imply the proceeding pulleys.

If the weight of the cable and friction force is assumed to be ignored, the driving parts connected by the motors are expressed as follows

$$J_m\ddot{\theta}_m+B_m\dot{\theta}_m+R_m\overline{T}_{m1}(R_m\theta_m-R_1\theta_1)=u_m \quad (1)$$

$$J_L\ddot{\theta}_L+B_L\dot{\theta}_L+R_L\overline{T}_{L3}(R_L\theta_L-R_3\theta_3)=u_L \quad (2)$$

where, u is the input torque from motors. J and B are the inertia and damping values of the pulley parts. R is the radius of the pulleys. $\overline{T}$ is the function of the difference in tension, which acts to transmit the force to the connected pulleys. In the real system, the influence of friction is considerable and the effort to understand and estimate the effect has been conducted.[18,20] However, the friction force has to be shown as torque in the driven model and the torque type friction modeling is difficult because normal force needed for Coulomb model is changeable as magnitude and direction of tension varies. So, this paper assumes ideal state regardless of friction in this stage. This issue will be our major topic in the future study, probably by employing similar approach found in Ref. 21. The difference in tension is generated by cable elongation, which is the disparity in circumferential length between two pulleys. Hook's law can be used to describe the tension with angular movement as follows:

$$\overline{\mathrm{T}}(\delta)=K(\delta)\bullet\delta \quad (3)$$

where K is the spring rate and δ is the elongation. In the linear elastic region in the strain-stress characteristics of a material, K can be regards as constant. However, K was related to δ here as a function of the yielding state; this can include all states as nonlinear elastic and a few yielding states as well as linear states.

At pulley 1, the dynamic equation has to consider not only the movement of pulley M and the end-effector of pulley 2 but also the coupled motion of pulley 3; this is expressed as follows:

$$J_1\ddot{\theta}_1+B_1\dot{\theta}_1+R_1\overline{T}_{12}(R_1\theta_1-R_1\theta_3-R_2\theta_2)=R_1\overline{T}_{m1}(R_m\theta_m-R_1\theta_1) \quad (4)$$

At pulley 2, the working force on end-effector F is included in the dynamic equation.

$$J_2\ddot{\theta}_2+B_2\dot{\theta}_2+LF=R_2\overline{T}_{12}(R_1\theta_1-R_1\theta_3-R_2\theta_2) \quad (5)$$

At pulley 3, coupled forces from Pulley 1 appear in the dynamic equation as follows.

$$J_3\ddot{\theta}_3+B_3\dot{\theta}_3+R_1\overline{T}_{12}(R_1\theta_1-R_1\theta_3-R_2\theta_2)=R_3\overline{T}_{l3}(R_L\theta_L-R_3\theta_3) \quad (6)$$

2.3 Cable characteristics

The cable for surgical robot instruments is pre-extended to reduce elongation.[15] Compared with a general wire, a pre-extended cable has a narrow linear elastic region and shows nonlinear characteristics in the strain-stress curve of a tension test. Thus, instead of a constant spring coefficient, the spring rate function, including nonlinearity, has to be derived using a tension test. The strain-stress characteristic of a general cable used in surgical robot instruments was examined by using a tension test machine as shown in Fig. 7. The results were used to determine the spring rate function K in (3).

Prolonged cycling of the cables can bring about hysteresis, which causes the slacking phenomenon in a cable system. However, pre-extended cables have a higher yielding point. The general grasping force of a human is about 6 kgf.[19] Repeated extension and release in the experimental test showed that less than 1% deformation is caused by hysteresis up to 20kgf. Thus this paper proposes that the spring rate function can be derived by sampling the tensile force-elongation test results up to 20 kgf to derive a look-up Table.

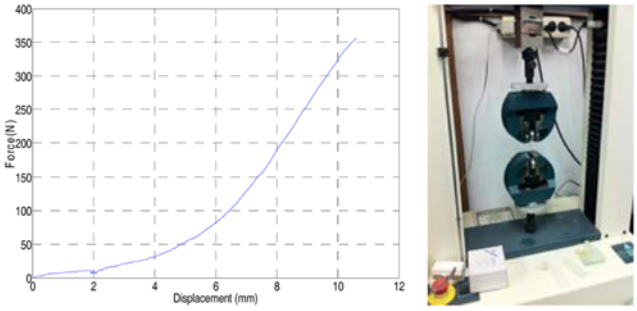

Fig. 7 Cable extension test result and test figure

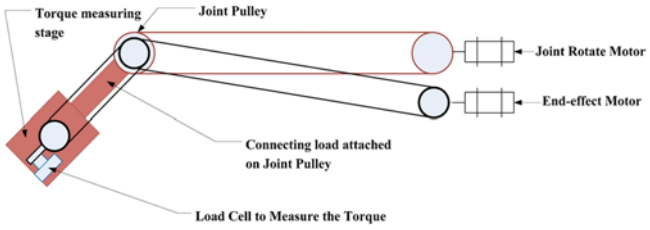

Fig. 8 Experimental system architecture

3. Proposed Method Evaluation

The specific behavior of a cable-driven surgical robot instrument is presented here. The governing equation proposed in this paper was simulated, and the proposed model was evaluated via simulation and experiment. First, experimental test equipment was designed and built to realize a representative cable-driven model for surgical robot instruments, as shown in Fig 8. The design shown in Fig. 8 is based on Fig. 6, which was used to derive the governing equation in this paper. Similar to surgical instruments, the two motor-driving pulley parts were designed to be separated by long distances from the other pulleys, as shown in Fig. 9. Thus, the elastic and cable material characteristics are extended to show them clearly. As shown in Fig. 9, the experimental test equipment consists of a screw handle to adjust the pretension between motor pulleys and link joints. The operating force on the end-effector was measured using load cell installed on the end-effect link, as shown in Fig. 9(a). Equipment specification is organized on Table 1.

3.1 Propagation and equilibrium

To examine the driving behavior of each pulley in the tendon-driven system of a surgical robot instrument, a simulation test was performed based on the governing equation derived in the second section. The

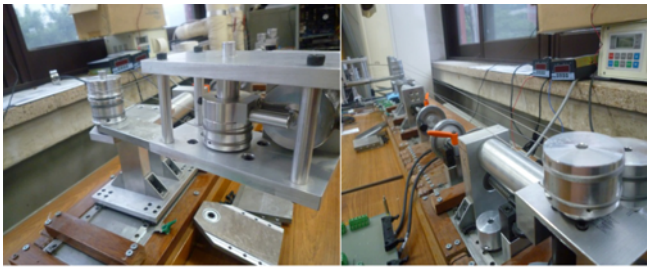

(a) (b)

Fig. 9 Experimental system: (a) Joint pulley and end-effector torque measuring system, (b) Two actuators

Table 1 Experimental Test System Properties

Part	Properties
Radius of Pulley M, L, 1, 2, 3	30 mm
Inertia of Pulley M, L, 1, 2	2.25×10^{-4} Kg·m
Inertia of Pulley 3	4×10^{-2} Kg·m
Cable	SAVA Low-Stretch High-Fatigue Miniature Stainless Steel Cable 1027
Arm length of End-effector	50
Motor	Maxon DC Motor 328331

Runge-Kutta method was applied to Eqs. (1)~(6) based on the system design properties shown in Table 1. The simulation results showed tension propagation and the interference phenomenon during the driving pulley's operation.

In the first simulation, a step input of 1° was applied to pulley M, and simultaneously, pulley L was controlled for keeping 0°. Fig. 10 shows the tension propagation between the middle pulleys: pulley 1 and 2. Although real surgical robot instruments move as a rigid body structure for high pre-tension and the delay response for the force propagation is not shown, simulation tests can show the transition period as shown in Fig 10. The results showed that the elastic characteristics of the cable tension cause vibrations. Although the B value in the model equation was considered as 0.9, the elastic characteristics affect the whole system more than the viscous term. The stronger the elastic effect of tension is, the less sui Table the cable is for surgical robot instrument. So many systems are designed to minimize the effect of the elastic characteristics. In our case, we minimize this by applying pre-tension to the cable and limiting the working range under 15 Kgf. Therefore, the effect of vibration is not a major factor in our design. Further, interference of the pulleys in series (pulleys 1 and 3) showed unexpected rotating angle results. The final rotation of the end-effector pulley 2 was performed by a combination of the two middle pulley rotations. However, elastic deformationelongation of the cable led to an error in the end-effector despite there being no error in the driving pulley. Thus, to eliminate the final end-effector control error, not only the initial tension of cables directly connected to end-effector but also those of all pulleys arranged in series and sharing the same axis, needed to be adjusted.

The second simulation test investigated the inner states of the system when the end-effector contacts some wall or grasps something and induces a force.

The test conditions were set by applying a step input of 6° to the

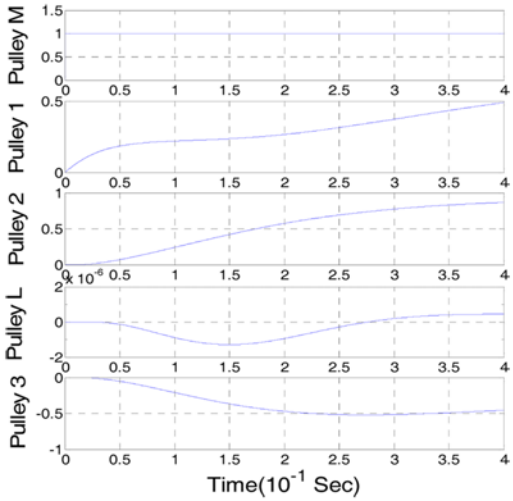

Fig. 10 Simulation test result for step input of 1°

end-effector driving pulley M and regulating the link-driving pulley L to 0°. The end-effector was blocked at 5°. Thus, the remaining 1° could be compensated for by the operating force on the end-effector. The simulation results are shown in Fig. 11.

The reaction force on the end-effector affected the link pulley partpulleys 3 and Lby interference. The elastic characteristics caused some vibration in the transient state. The system then finally reached the force equilibrium states. The operating force on end-effector was estimated to be 1.83 N. The results showed that the operating force on end-effector was determined by the equilibrium states of the pulleys connected in series as well as those driven directly. Moreover, the operating force appeared to be affected by the elastic characteristics of connected cables within the pulleys.

3.2 Operating force estimation

A major contribution of this paper is that the proposed governing equation can estimate the operating force on the end-effector which is still hard to measure for surgical robot instruments. Therefore, this study attempted to estimate the force with the position control of the driving motors. The estimated value based on the governing equation was compared with experimental test results for validation.

Fig. 12 shows the input trajectory of end-effect driving pulley M. The link pulley L is controlled to be a 0° regulator. In the experimental test, the end-effector was set to reach the load cell to measure the operating force and fix the position. Fig. 13 shows the estimated operating force which was generated by numerical analysis applied to the derived model with Runge-Kutta method. The estimated operating force is shown in Fig. 13 according to the experimental test system. The initial peak force was about 18 N at 5°. At 7° it increases up to 50 N. When returning to 5°, the force is less than that in initial condition. At 4°, the force quickly decreases.

Fig. 14 shows the experimental test result. The conventional low gain PID was used to prevent the cable from snapping because the allowable tension is only 15 Kgf. However, this means that tracking error is bound to occur. At the beginning, the force increased to 18 N. However, during the second increase period, pulley 3 quickly turned because of the movement of pulley M. The reason for the error was the

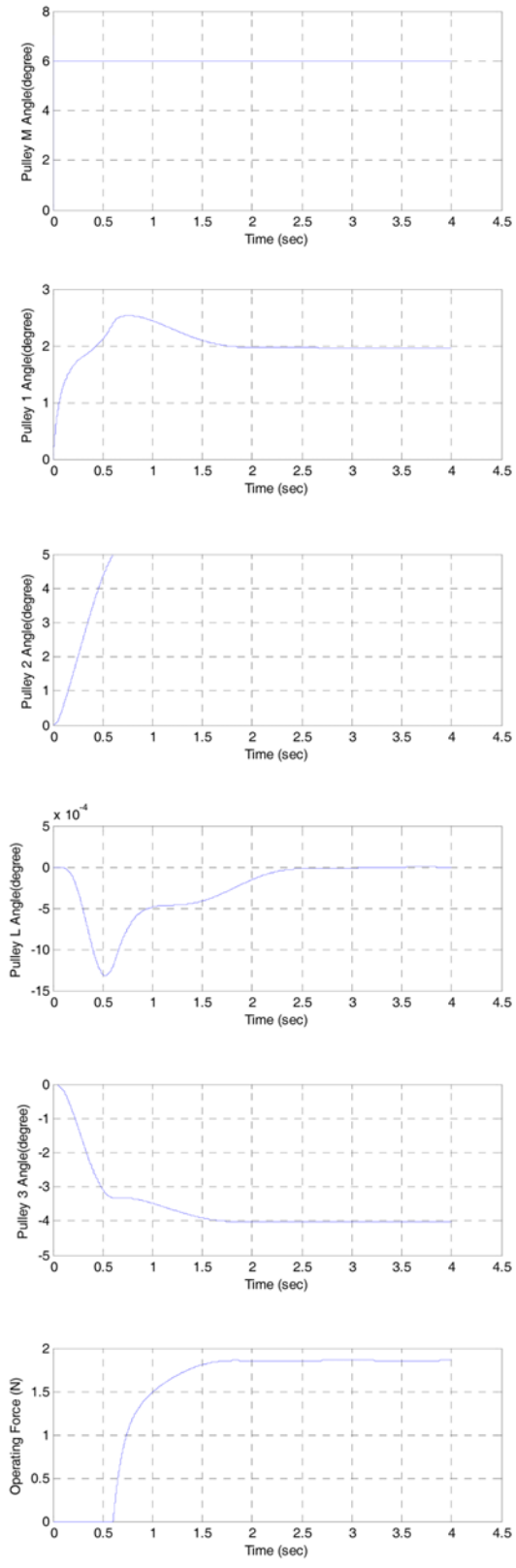

Fig. 11 Simulation test result for operating force effect

difference in initial tensions between pulleys M and 1 and pulleys L and 3. The tension from pulleys M to 1 was much more than that from pulleys L to 3. The reaction force was unexpectedly absorbed by the loose cable part.

Unfortunately, the actuator part mounting pulleys L and M was

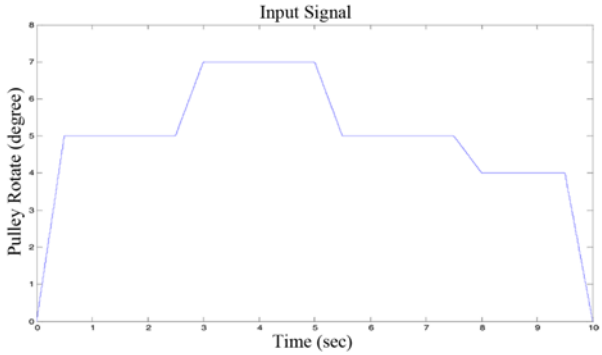

Fig. 12 Input trajectory of pulley M

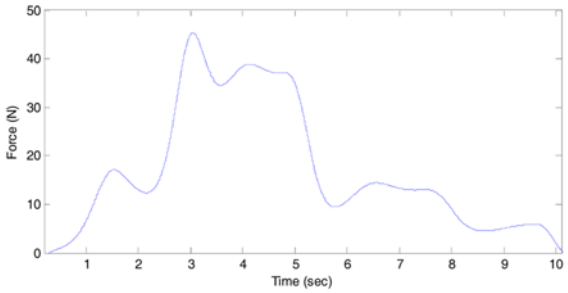

Fig. 13 Estimated operating force of end-effect on Pulley 2 link

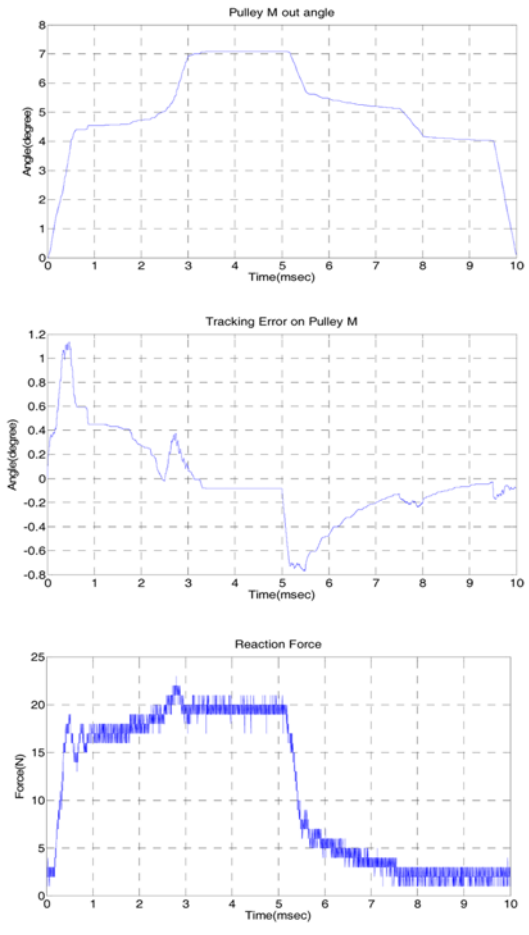

Fig. 14 Experimental test results on test system

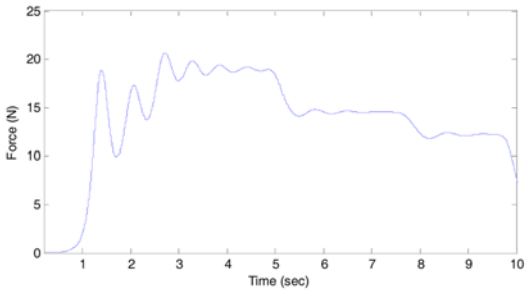

Fig. 15 Estimated operating force of end-effect on pulley 2 link after adjusting pretension

produced in one body; the same held true for pulleys 1 and 3. Thus, the tension-adjusting equipment cannot control the tension separately. However, at the beginning when the reaction force was small and not much tension propagation to the series pulley occurred, the estimated force was similar to the estimated values calculated by the proposed governing equation. But the estimated force was different from the middle of experiment test. As the base design is not easy to be changed instead of solving the deficiency of independently tension adjustment in mock-up experimental system, this paper proves the assertion by reversely numerical analysis simulation repeated based on the lower pretension value, especially at the 10% lower pretension between L and 3 than between 1 and M. The friction effect was considered for the practicality. The friction torque was assumed as opposite direction to the velocity and proportional to tension. Fig. 15 shows the estimating result after adjusting the pretensions. Until 5 sec, the estimating force is similar with real experimental test result. However, the static friction between the joint pulley and the stand plate shown in Fig. 9(a) governed the system and there occurred large difference between estimation and test result after 5 sec. When the friction model is adopted to improve the estimation error in the next study, this difference will decrease. From the results, the proposed governing equation is correct, which suggests that the spring rate function of the cable material characteristic in the working region and derived governing equation, including interference in the coupled link, can be used to estimate the operating force on the system.

4. Conclusion

In this paper, a dynamic governing model of a coupled cable pulley structure for use in surgical robot instruments was derived. The dynamic model shows the coupled motion, interference within series pulleys sharing an axis, and operation force inclination after tension equilibrium within all cables occurred. In particular, a spring rate function for cable material characteristics is proposed and applied to a governing equation. The operating force on end-effector, for which there are still difficulties with measurement in surgical robot instruments, can be estimated and was found to be similar to actual values through a comparison with experimental test values, although the experimental equipment has a design fault; hence, the entire process could not be shown clearly. The dynamic analysis presented in this paper shows that the operating force is affected by the elastic characteristics of connected cables within the pulleys and can be estimated by the proposed method. Thus if the pretension of commercialized surgical robot instruments is known and adjusTable, the force can be estimated by applying the proposal in this paper. The proposed dynamic analysis also makes precision control of the end-effector possible.

ACKNOWLEDGEMENT

This research was supported by Basic Science Research Program through the National Research Foundation of Korea (NRF) funded by the Ministry of Education, Science and Technology (2011-0014915) and supported by the National Research Foundation of Korea (NRF) grant funded by the Korea government (MSIP) (No. NRF-2012M2B2B 1055503).

REFERENCES

1. Baker, S., Nisar, A., Paice, A., and Abdulaal, Y., “Laparoscopic-Assisted Enteroscopy,” Annals of The Royal College of Surgeons of England, Vol. 92, No. 3, pp. W4-W6, 2010.
2. Giulianotti, P. C., Coratti, A., Angelini, M., Sbrana, F., Cecconi, S., et al., “Robotics in General Surgery: Personal Experience in a Large Community Hospital,” Archives of Surgery, Vol. 138, No. 7, pp. 777-784, 2003.
3. Riza, E. D., “Laparoscopic Surgical Instrument,” US Patent, No. 5480409A, 1996.
4. Vidal, C. A., Plylet, A. K., Redmond, R. J., and Lagerquist, R., “Surgical Instrument Having an Articulated Jaw Structure and a Detachable Knife,” US Patent, No. 5749893A, 1998.
5. Kuehn, S. T. and Montpetit, K. P., “Devices with a Bendable Tip for Medical Procedures,” US Patent, No. 6743239B1, 2004.
6. Reyes, D. A. G., Tang, B., and Cuschieri, A., “Minimal Access Surgery (Mas)-Related Surgeon Morbidity Syndromes,” Surgical Endoscopy and Other Interventional Techniques, Vol. 20, No. 1, pp. 1-13, 2006.
7. Horgan, S. and Vanuno, D., “Robots in Laparoscopic Surgery,” Journal of Laparoendoscopic & Advanced Surgical Techniques, Vol. 11, No. 6, pp. 415-419, 2001.
8. Kobayashi, Y., Chiyoda, S., Watabe, K., Okada, M., and Nakamura, Y., “Small Occupancy Robotic Mechanisms for Endoscopic Surgery,” Proc. of Medical Image Computing and Computer-Assisted Intervention, pp. 75-82, 2002.
9. Abbott, D. J., Becke, C., Rothstein, R. I., and Peine, W. J., “Design of an Endoluminal Notes Robotic System,” Proc. of IEEE/RSJ International Conference on Intelligent Robots and Systems, pp. 410-416, 2007.
10. Intuitive Surgical, “EndoWrist Instruments,” http://www.intuitivesurgical.com/products/instruments/ (Accessed 14 AUG

2014)

11. Chalon, M., Wimbock, T., and Hirzinger, G., "Torque and Workspace Analysis for Flexible Tendon Driven Mechanisms," Proc. of IEEE International Conference on Robotics and Automation (ICRA), pp. 1175-1181, 2010.
12. Marcheschi, S., Frisoli, A., Avizzano, C. A., and Bergamasco, M., "A Method for Modeling and Control Complex Tendon Transmissions in Haptic Interfaces," Proc. of IEEE International Conference on in Robotics and Automation, pp. 1773-1778, 2005.
13. Prisco, G. M. and Bergamasco, M., "Dynamic Modelling of a Class of Tendon Driven Manipulators," Proc. of 8th International Conference on Advanced Robotics, pp. 893-899, 1997.
14. Yin, X. and Bowling, A. P., "Dynamic Performance Limitations due to Yielding in Cable-Driven Robotic Manipulators," Journal of Mechanical Design, Vol. 128, No. 1, pp. 311-318, 2006.
15. Carl Stahl Sava Industries, Inc, "Design Guide for Cable Solutions," http://www.savacable.com/sava_cat.pdf (Accessed 19 SEP 2014)
16. Kim, C. Y., Lee, M. C., Lee, T. K., Choi, S. W., and Park, M. K., "Study for the Indirect Measuring Method of Operational Force in Surgical Robot Instrument," Journal of Institute of Control Robotics and Systems, Vol. 16, No. 9, pp. 840-845, 2010.
17. Bodner, J., Wykypiel, H., Wetscher, G., and Schmid, T., "First Experiences with the Da Vinci Operating Robot in Thoracic Surgery," European Journal of Cardio-Thoracic Surgery, Vol. 25, No. 5, pp. 844-851, 2004.
18. Lee, T. K., Kim, C. Y., and Lee, M. C., "Friction Analysis According to Pretension of Laparoscopy Surgical Robot Instrument," Int. J. Precis. Eng. Manuf., Vol. 12, No. 2, pp. 259-266, 2011.
19. National Aeronautics and Space Administration, "Human Performance Capabilities," in: Man-Systems Integration Standards, Vol. 1, Sec. 4, 4.9.3(A), 1995.
20. Mahvash, M. and Okamura, A., "Friction Compensation for Enhancing Transparency of a Teleoperator with Compliant Transmission," IEEE Transactions on Robotics, Vol. 23, No. 6, pp. 1240-1246, 2007.
21. Yoon, S. M., Lee, M. C., Kim, C. Y., and Kang, B. H., "Evaluation of a Possibility of Estimation of Reaction Force of Surgical Robot Instrument using Sliding Perturbation Observer," Journal of Korea Robotics Society, Vol. 7, No. 1, pp. 20-28, 2012.